Clutter Filter Design for Ultrasound Color Flow Imaging

by

Steinar Bjærum   (Corresponding author)
Department of Physiology and Biomedical Engineering
Norwegian University of Science and Technology
Trondheim, Norway

Mail adress:
GE Vingmed Ultrasound
P.O. Box 141
N-3191 Horten
Norway
e-mail: steinarb@medisin.ntnu.no
Tel.: +47 33 02 11 10
Fax: +47 33 02 13 57

Hans Torp
Department of Physiology and Biomedical Engineering
Norwegian University of Science and Technology
Trondheim, Norway

Kjell Kristoffersen
GE Vingmed Ultrasound
Horten, Norway

Abstract

To get ultrasound color flow images of high quality, it is important to sufficiently suppress the clutter signals originating from stationary and slowly moving tissue. Without sufficient clutter rejection, low velocity blood flow can not be measured, and estimates of higher velocities will have a large bias. The small number of samples available (8-16) makes clutter filtering in color flow imaging a challenging problem. In this paper we review and analyze three classes of filters: FIR, IIR, and regression filters. The quality of the filters was assessed based on the frequency response, as well as on the bias and variance of a mean blood velocity estimator using an autocorrelation technique. For FIR filters, the frequency response was improved by allowing a non-linear phase response. By estimating the mean blood flow velocity from two vectors filtered in the forward and backward direction, respectively, the standard deviation was significantly lower with a minimum phase filter than with a linear phase filter. For IIR filters applied to short signals, the transient part of the output signal is important. We analyzed zero, step, and projection initialization, and found that projection initialization gave the best filters. For regression filters, polynomial basis functions provide effective clutter suppression. The best filters from each of the three classes gave comparable bias and variance of the mean blood velocity estimates. However, polynomial regression filters and projection initialized IIR filters had a slightly better frequency response than could be obtained with FIR filters.

1   Introduction

In ultrasound Doppler blood flow measurements, the signal scattered from blood is corrupted by signals scattered from muscular tissue such as vessel walls, etc. This clutter signal is typically 40-100dB stronger than the signal from blood. The signal scattered by the rapidly moving blood cells has a larger Doppler frequency shift than the signal reflected from slowly moving tissue. A high-pass filter can therefore be used to separate the signals from blood and tissue. To get adequate frame rates in 2D color flow imaging, only $8 - 16$ samples are generally available for high-pass filtering. While there are many conventional filter design techniques, all these algorithms consider only the steady state frequency response. For the short signals available in color flow imaging, the transient response is significant, and the steady state response can not

be used to compare the filters. In this paper we analyze IIR filters with various initialization techniques [1, 2, 3], FIR filters with and without a linear phase response [4], and regression filters [5, 3, 6] in order to determine which filter is best for clutter filtering in color flow imaging. The paper considers more filter types and goes deeper into the design procedure than previous papers have done [7, 8, 3].

It has been suggested to adapt the clutter filter to the tissue movement by down-mixing the signal with the estimated mean tissue frequency [9]. This paper does not consider such an adaptation to the tissue movement, but down-mixing can be done prior to all the filters considered. Paper [8] suggests initializing an IIR filter to suppress the transient from a complex exponential with frequency equal to the estimated mean frequency. This is called exponential initialization, and results in a non-linear filter and is not considered in this paper. The approach, however, seems similar to down-mixing with the mean frequency prior to a step-initialized IIR filter.

The paper is organized as follows. General theory for linear clutter filters is presented in Section 2. In Sections 3, 4, and 5, FIR, IIR, and regression filters are presented, respectively. Different filters within each of the filter classes are analyzed and compared. The best filters from each class are compared in Section 6, while Section 7 contains the final discussion and conclusions.

2   General Linear Clutter Filters

A 2D color flow imaging system scans the ultrasound beam over the region to be imaged, transmits N pulses in each direction, and estimates the blood flow velocities from the backscattered signals. The number of pulses N will be referred to as the packet size. A well established technique is to estimate the blood flow velocities based on the temporal samples of the complex demodulated signal from fixed positions in space. The clutter filter thus operates on a one-dimensional signal consisting of N temporal samples.

It is convenient to organize the N samples of the complex demodulated Doppler signal in a vector $\mathbf{x} = [x(0), x(1), \ldots, x(N-1)]^T$. A general one-dimensional clutter rejection filter can be described mathematically as a transform on the N-dimensional complex vector space $\mathbb{C}^N$.

Restricting the treatment to linear filters, a general linear filtering operation can be expressed by the matrix multiplication

$$\mathbf{y} = \mathbf{A}\mathbf{x} \tag{1}$$

where $\mathbf{A}$ is an $M \times N$ matrix, and the output vector $\mathbf{y} = [y(0), y(1), \ldots, y(M-1)]^T$ has dimension M. With the matrix element in row n and column k denoted by $a(n, k)$, the elements of the output vector are given by

$$y(n) = \sum_{k=0}^{N-1} a(n, k)x(k), \quad n = 0, \ldots, M - 1 \tag{2}$$

The filter is linear, but not generally time invariant. It is therefore not possible to define the frequency response as the Fourier transform of an impulse response. For a general linear filter, the frequency response is defined as the power of the output signal when the input is a complex harmonic signal [6] with unit amplitude. A discrete-time complex exponential is defined by

$$x(k) = e^{jk\omega}, \quad k = 0, \ldots, N - 1 \tag{3}$$

where $\omega \in [-\pi, \pi]$ is the normalized frequency, and $j = \sqrt{-1}$. With this input signal, the output becomes

$$y_\omega(n) = \sum_{k=0}^{N-1} a(n, k)e^{jk\omega} = A_n(-\omega), \quad n = 0, \ldots, M - 1 \tag{4}$$

where $A_n(\omega)$ is the Fourier transform of row n. The frequency response then becomes

$$H_0(\omega) = \frac{1}{M} \sum_{n=0}^{M-1} |y_\omega(n)|^2 = \frac{1}{M} \sum_{n=0}^{M-1} |A_n(-\omega)|^2 \tag{5}$$

The parameters describing the frequency response of a high pass filter are illustrated in Figure 1. The stopband is limited by the stopband cut off frequency ω_s, which should be large enough to remove the clutter signal. The deviation from zero in the stopband is given by d_s, which should be as small as possible to get sufficient clutter rejection. In the passband, all the frequencies should be passed through unaltered which means that d_p should be minimized. Finally, the passband cut off frequency ω_p should be as close as possible to ω_s. This ensures that a maximal range of blood velocities can be measured.

3   Finite Impulse Response (FIR) Filters

As the name implies, the impulse response of an FIR filter is of finite length. The output of a $(K-1)^{\text{th}}$ order FIR filter can therefore be written as the finite convolution sum

$$y(n) = \sum_{k=0}^{K-1} h(k)x(n-k) = \sum_{k=n-K+1}^{n} h(n-k)x(k) \tag{6}$$

The output is not valid until all the filter registers are filled up with input data. With packet size N, and filter order $K-1$, the number of valid output samples is $N-K-1$. It can be shown that for FIR filters, the frequency response defined in Equation 5 becomes $H_0(\omega) = |H(\omega)|^2$, where $H(\omega)$ is the Fourier transform of the impulse response $h(n)$.

3.1   FIR Filters with Linear Phase

A filter has linear phase if the frequency response can be written

$$H(\omega) = G(\omega)e^{j(k_1+k_2\omega)} \tag{7}$$

where $G(\omega)$ is a real function, and k_1 and k_2 are constants. The advantage of linear phase is that in the passband, the frequency response is $H(\omega) \sim e^{j(k_1+k_2\omega)}$. For a signal $x(n)$ consisting only of frequencies in the passband of the filter, the spectrum of the filtered signal is $Y(\omega) \sim X(\omega)e^{j(k_1+k_2\omega)}$. This is just a constant phase shift and a time delay of the input signal, and the wave form is not distorted. An FIR filter with real coefficients has linear phase if the impulse response satisfies the symmetry constraint

$$h(n) = \pm h(K-n-1) \tag{8}$$

Many design techniques exist for linear phase FIR filters [4], but we will only consider the design of equiripple filters using the McClellan-Parks algorithm. The maximum deviation from the desired stop- and passband response is minimized, and filters designed with this algorithm are optimal in the *minimax* sense [4].

3.2   FIR Filters with Minimum Phase

Linear phase imposes a symmetry constraint on the impulse response as shown in Equation 8. Without any phase constraints, the required order to obtain a specified amplitude response is

4

expected to be reduced. FIR filters with optimum amplitude response in the *minimax* sense can be designed as described in [10]. Since only the amplitude response is considered, many filters with the optimum amplitude response but different phase responses exist. Among these filters, the minimum phase filter has all the zeros inside the unit circle, and has the smallest time delay [11]. The minimum phase filter also maximizes the partial energy $E(n) = \sum_{k=0}^{n} |h(k)|^2$ of the impulse response [11], and therefore has the most asymmetric impulse response.

Blood flow parameters are commonly estimated from an estimate of the autocorrelation function of the filtered signal [12]. For an FIR filter, the autocorrelation function of the output signal y is given by

$$R_y(m) = \frac{1}{2\pi} \int_{-\pi}^{\pi} S_x(\omega)|H(\omega)|^2 e^{jm\omega} d\omega \tag{9}$$

when the input signal x has power spectrum $S_x(\omega)$. Since $R_y(m)$ is independent of the phase response of the filter, it is safe to disregard the phase response when designing FIR clutter filters for use together with autocorrelation estimates. The minimum phase filter has a highly asymmetric impulse response function, and the input samples are weighted differently if the impulse response is reversed. The variance might therefore be reduced if the autocorrelation estimate is calculated from two output vectors filtered in the forward and backward direction, respectively. This is investigated in Section 6.

3.3   Comparison of Linear and Minimum Phase FIR Filters

When designing both linear- and minimum phase FIR filters, the following parameters defined in Figure 1 were specified:

- Maximum filter order.

- Minimum stopband cut off frequency, ω_s.

- Maximum stopband ripple, d_s.

- Maximum passband ripple, d_p.

With these parameters specified, the minimum passband cut off frequency ω_p was calculated. When the minimum ω_p was found, d_s was minimized without altering the other quantities. Table 1 shows an example of the filter parameters obtained for linear and minimum phase FIR

5

filters of order 5. The corresponding frequency responses are shown in Figure 2, where we see that the passband cut-off frequency decreases from 0.58π to 0.49π when a non-linear phase is allowed. Filters with minimum phase will therefore be used when FIR filters are compared to other filter classes.

4 Infinite Impulse Response (IIR) Filters

A Kth order infinite impulse response (IIR) filter is described by the difference equation

$$y(n) = -\sum_{k=1}^{K} a_k y(n-k) + \sum_{k=0}^{K} b_k x(n-k) \tag{10}$$

where we see that each output sample depends on present and past input samples, as well as past output samples. The recursive part of the filter causes the response to an impulse input to endure forever, and is the reason why such filters are called IIR filters.

4.1 Steady State and Transient Response

There are many techniques for designing IIR filters based on the steady state magnitude response. The most common IIR filters are Butterworth, Chebyshev type I and II, and Elliptic filters. A summary of the properties of these filters can be found in [13]. With an input signal of finite length, the transient response becomes important. Examples of the transient signal for a sinusoidal signal input to Butterworth, Chebyshev, and Elliptic high pass filters of order 3 are shown in Figure 3. The Butterworth filter has the smallest transient since among the three filter types, Butterworth filters have poles with the smallest magnitude. Butterworth filters have a wider transition region than the other filters, and there is thus a trade-off between transient duration and magnitude response.

4.2 State Space Formulation

To investigate different techniques for reducing the transient shown in Figure 3, a state space formulation [11] of the IIR filter will be convenient. The state vector is defined by $\mathbf{v}(n) = [v_1(n)\ v_2(n)\ \ldots\ v_K(n)]^T$ where $v_i(n)$ is the content of filter memory register i in the direct form II implementation of the filter [11]. The filter is then described by the following state space

6

equations

$$\mathbf{v}(n+1) = \mathbf{F}\mathbf{v}(n) + \mathbf{q}x(n) \tag{11}$$

$$y(n) = \mathbf{g}^T\mathbf{v}(n) + dx(n) \tag{12}$$

where the elements of $\mathbf{F}$, $\mathbf{q}$, $\mathbf{g}$, and d are

$$\mathbf{F} = \begin{bmatrix} 0 & 1 & 0 & \cdots & 0 \\ 0 & 0 & 1 & \cdots & 0 \\ \vdots & \vdots & \vdots & & \vdots \\ 0 & 0 & 0 & \cdots & 1 \\ -a_K & -a_{K-1} & -a_{K-2} & \cdots & -a_1 \end{bmatrix}, \quad \mathbf{q} = \begin{bmatrix} 0 \\ 0 \\ \vdots \\ 0 \\ 1 \end{bmatrix}$$

$$\mathbf{g} = \begin{bmatrix} b_K - b_0 a_n \\ b_{K-1} - b_0 a_{K-1} \\ \vdots \\ b_1 - b_0 a_1 \end{bmatrix}, \quad d = b_0 \tag{13}$$

Let the input and output sequences be viewed as $N \times 1$ vectors, $\mathbf{x} = [x(0)\ x(1)\ \ldots\ x(N-1)]^T$, and $\mathbf{y} = [y(0)\ y(1)\ \ldots\ y(N-1)]^T$. The relationship between the input and output of the filter can then be written as the matrix-vector equation

$$\mathbf{y} = \mathbf{B}\mathbf{v}(0) + \mathbf{C}\mathbf{x} \tag{14}$$

where

$$\mathbf{B} = \begin{bmatrix} \mathbf{g}^T \\ \mathbf{g}^T\mathbf{F} \\ \vdots \\ \mathbf{g}^T\mathbf{F}^{N-1} \end{bmatrix}, \quad \text{and} \quad \mathbf{C} = \begin{bmatrix} d & 0 & \cdots & 0 & 0 \\ \mathbf{g}^T\mathbf{q} & d & \cdots & 0 & 0 \\ \vdots & \vdots & & \vdots & \vdots \\ \mathbf{g}^T\mathbf{F}^{N-2}\mathbf{q} & \mathbf{g}^T\mathbf{F}^{N-3}\mathbf{q} & \cdots & \mathbf{g}^T\mathbf{q} & d \end{bmatrix} \tag{15}$$

We will now investigate different ways $\mathbf{v}(0)$ can be chosen to minimize the transient.

4.3   Zero Initialization

The initial filter state vector is set equal to the zero vector, $\mathbf{v}(0) = \mathbf{0}$. This is equivalent to assuming that the input signal is identical to zero for $n < 0$. The filtering operation is equal to

$$\mathbf{y} = \mathbf{C}\mathbf{x} \tag{16}$$

where $\mathbf{C}$ is given in Equation 15.

4.4   Step Initialization

The transient response depends on the input signal and can not be removed unless the input signal is completely known. However, the transient can be partially suppressed by using the a priori knowledge available about the input signal. In color flow imaging, the input signal is dominated by the low frequency clutter signal. The input signal is therefore assumed to have a constant value equal to the first signal sample $x(0)$. For a stable filter, the transient dies out with time, and for a step input, the filter registers converge to constant values. The transient can thus be suppressed by setting the initial filter state equal to the state an infinitely long time after the step is applied at the input. This initial filter state is found by utilizing the final value theorem of the one-sided $\mathcal{Z}$-transform [11]. Transformation of Equation 11 gives

$$\mathbf{V}^+(z) = z(z\mathbf{I} - \mathbf{F})^{-1}\mathbf{v}(0) + (z\mathbf{I} - \mathbf{F})^{-1}\mathbf{q}X^+(z) \tag{17}$$

and the transform of the assumed input step signal is given by $x(0)z/(z-1)$. The initial state of the filter is then given by

$$\begin{aligned} \mathbf{v}_{step}(0) &= \lim_{z \to 1}(z-1)\left(z(z\mathbf{I} - \mathbf{F})^{-1}\mathbf{v}(0) + (z\mathbf{I} - \mathbf{F})^{-1}\mathbf{q}\frac{x(0)z}{z-1}\right) \\ &= x(0)(\mathbf{I} - \mathbf{F})^{-1}\mathbf{q} \end{aligned} \tag{18}$$

Inserting this in Equation 14 the filter with step initialization is given by

$$\mathbf{y} = \left(\mathbf{B}(\mathbf{I} - \mathbf{F})^{-1}\mathbf{q}\mathbf{1} + \mathbf{C}\right)\mathbf{x} \tag{19}$$

where $\mathbf{1}$ is the $1 \times N$ vector $[1\ 0\ \cdots\ 0]$.

4.5   Projection Initialization

The transient part of the output signal is of the same form as the response with just a zero input signal [2]. By setting $\mathbf{x} = \mathbf{0}$ in Equation 14 we see that the transient is in the subspace spanned by the columns of the matrix $\mathbf{B}$. The projection matrix $\mathbf{P}_B = \mathbf{B}(\mathbf{B}^T\mathbf{B})^{-1}\mathbf{B}^T$ is the projection into this transient subspace [2]. The component of the output signal in the transient subspace is removed by forcing $\mathbf{P}_B\mathbf{y} = \mathbf{0}$. This is obtained by the following initial state vector

$$\mathbf{v}(0) = -(\mathbf{B}^T\mathbf{B})^{-1}\mathbf{B}^T\mathbf{C}\mathbf{x} \tag{20}$$

8

Inserting this in Equation 14 the filter with projection initialization is given by

$$\mathbf{y} = (\mathbf{I} - \mathbf{B}(\mathbf{B}^T\mathbf{B})^{-1}\mathbf{B}^T)\mathbf{C}\mathbf{x} \qquad (21)$$

4.6 Mirroring of the Input Sequence

The transient decays with time, and the effect of the transient can be reduced by discarding some of the first output samples. This reduction in the number of output samples, however, increases the variance when estimating flow parameters. A better approach is to "increase" the input signal length based on the available samples and then discard the first output samples. One way to obtain this is to mirror the input vector around the first sample, producing the $2N-1$ dimensional vector $\mathbf{x}_m$ as shown in Figure 4. Mathematically, this mirroring is expressed by the $(2N-1) \times N$ matrix $\mathbf{M}_1$:

$$\mathbf{x}_m = \mathbf{M}_1\mathbf{x}, \quad \text{where} \quad \mathbf{M}_1 = \begin{bmatrix} 2 & 0 & \cdots & 0 & -1 \\ 2 & 0 & \cdots & -1 & 0 \\ \vdots & \vdots & \cdots & \vdots & \vdots \\ 2 & -1 & \cdots & 0 & 0 \\ 1 & 0 & \cdots & 0 & 0 \\ 0 & 1 & \cdots & 0 & 0 \\ \vdots & \vdots & \cdots & \vdots & \vdots \\ 0 & 0 & \cdots & 0 & 1 \end{bmatrix} \qquad (22)$$

The matrices in Equation 15 must be adjusted for an input vector of length $2N-1$, and give the output vector $\mathbf{y}_m$. The initial state vector $\mathbf{v}(0)$ is calculated based on $\mathbf{x}_m$. The final output vector $\mathbf{y}$ is the last N samples of $\mathbf{y}_m$. This selection of samples is obtained by the $N \times (2N-1)$ matrix $\mathbf{M}_2$:

$$\mathbf{y} = \mathbf{M}_2\mathbf{y}_m, \quad \text{where} \quad \mathbf{M}_2 = [\mathbf{0}_{N\times N-1} \ \mathbf{I}_{N\times N}] \qquad (23)$$

The entire filter including this mirroring operation is given by

$$\mathbf{y} = \mathbf{M}_2\mathbf{B}\mathbf{v}(0) + \mathbf{M}_2\mathbf{C}\mathbf{M}_1\mathbf{x} \qquad (24)$$

The matrix $\mathbf{M}_1\mathbf{B}$ has dimensions $N \times N$, while the matrix $\mathbf{M}_2\mathbf{B}$ has dimensions $N \times K$. The mirroring operation can be repeated several times, i.e. the mirrored input vector $\mathbf{x}_m$ can be mirrored to obtain a vector of length $4N-3$.

4.7 Comparison of Initialization Techniques

Examples of frequency responses for Butterworth, Chebyshev, and elliptic filters with different initialization techniques are shown in Figure 5. In this figure we see that for packet size $N = 8$, zero initialization results in insufficient stopband rejection. The step initialized filters have a zero at zero frequency, but the stopband is very narrow. The projection initialized filters have a stopband width equal to the steady state response, but with a wider transition region. Frequency responses for the Chebyshev filter when the input vector is mirrored are shown in Figure 6. Comparing the responses in Figure 6 with those in Figure 5, we see an improvement for zero- and step initialization. For projection initialization, however, mirroring results in a degradation of the response. From Figures 5 and 6, we can conclude that projection initialization without any mirroring of the input vector is the preferred initialization technique for IIR filters. Among the different IIR responses, the Chebyshev response is a good choice since it has a steep transition region and a monotonic stopband. An IIR Chebyshev filter with projection initialization will therefore be used when comparing IIR filters to other filter classes. The stopband width of a projection initialized Chebyshev filter can be increased either by increasing the order or the cut-off frequency of the steady state response. It is, however, not possible to get a significant increase in the -80dB stopband width by increasing the cut-off frequency, the only result is an undesirable widening of the transition region. A better approach is to increase the filter order while keeping the cut-off frequency low. This is illustrated in Figure 7. The frequency responses were also relatively independent of the passband ripple specified for the steady state response. A peak-to-peak ripple of 1dB was used in all the designs of IIR filters.

No symmetry properties can be stated for the rows of an IIR filter matrix. As for minimum phase FIR filters, there is thus a potential reduction of estimator variance if flow parameters are estimated based on two output vectors filtered in the forward and backward direction, respectively. This is investigated in Section 6.

5 Regression Filters

A regression filter calculates the best least-square fit of the signal to a set of curve forms modeling the clutter signal, and subtracts this clutter approximation from the original signal. The curve

forms span a subspace of the N-dimensional signal space which we call the clutter space. The best least-square fit is the projection of the signal into the clutter space, and the filter matrix is given by

$$\mathbf{A} = \mathbf{I} - \sum_{k=0}^{K-1} \mathbf{b}_k \mathbf{b}_k^{*T} \qquad (25)$$

where $\mathbf{b}_k$ is a set of orthonormal basis vectors spanning the K-dimensional clutter space, and $\mathbf{I}$ is the identity matrix. The frequency response is

$$H_0(\omega) = 1 - \frac{1}{N} \sum_{k=0}^{K-1} |B_k(\omega)|^2 \qquad (26)$$

where $B_k(\omega)$ is the Fourier transform of basis vector k [6]. We see from Equation 26 that to get a high pass filter, the basis vectors should be low-frequency functions. Conventional frequency analysis suggests using low-frequency sinusoids as basis vectors. The regression filter is then equivalent to calculating the Discrete Fourier Transform and then setting the low-frequency coefficients equal to zero prior to the inverse transform. An example of the obtained frequency response is shown with a dotted line in Figure 8, where we see that this basis does not provide sufficient stopband attenuation. There is a large distance between the zeros in the frequency response, and small attenuation between them. A better frequency response is obtained by increasing the sinusoidal period beyond the packet size. The frequency response when the period of the sinusoids is four times the packet size is shown with a solid line in Figure 8. The zeros come closer together with greater attenuation between them. In the limit, when the period of the sinusoids is increased, they become polynomials within the signal interval. An orthonormal basis is obtained by using the Legendre polynomials as basis vectors, and the resulting filter is called a polynomial regression filter [5, 3, 6]. Frequency responses for polynomial regression filters with different dimensions of the clutter space are shown in Figure 9a. The polynomial regression filters have a smooth and monotonic frequency response, and a polynomial basis for the clutter space will therefore be used when regression filters are compared to other filter classes. The frequency response of polynomial regression filters changes in discrete steps with clutter space dimension as seen in Figure 9a. The frequency response also varies with packet size. To obtain the same stopband width with a larger packet size, the clutter space dimension has to be increased.

Frequency responses in between those shown in Figure 9a can be obtained by using the filter

matrix

$$\mathbf{A} = \mathbf{I} - \sum_{k=0}^{K-1} c_k \cdot \mathbf{b}_k \mathbf{b}_k^{*T} \qquad (27)$$

where c_k are real constants. Examples of the resulting frequency responses are shown in Figure 9b for clutter space dimension equal to three, and $c_0 = c_1 = 1$ while c_2 was 0.25, 0.5 and 0.75 in the three examples shown. The -80dB stopband width is not significantly different from the regression filter with clutter space dimension equal to 2. The transition region is, however, significantly wider, and the best performance is obtained with the conventional polynomial regression filter in Equation 25.

The polynomial basis vectors $\mathbf{b}_k$ are either odd or even symmetric, $b(k) = \pm b(N - 1 - k)$. Using this property in Equation 25, the filter matrix elements satisfy $a(n, k) = a(N - 1 - n, N - 1 - k)$. Therefore, a reversal of the input vector only results in a reversal of the output vector. Thus no reduction in estimator variance is obtained by filtering in both the forward and backward direction.

6   Comparison of the Different Filter Classes

In the previous sections, the filters with best frequency responses within the FIR, IIR, and regression filter classes were found. Examples of frequency responses for these three filter classes are shown in Figure 10a for packet size $N = 8$ and in Figure 10b for packet size $N = 16$. The filters were designed with the parameters given in Table 2. These parameters were chosen to achieve filters with comparable frequency responses. The polynomial regression filters have frequency responses almost identical to the projection initialized IIR filters. This is expected since the output vector for both filters is projected into the orthogonal complement of a subspace with low frequency basis functions. The FIR filters have the widest transition regions, and is not the preferred choice based on the frequency response. Figure 10 also contains examples of the power spectra used in the simulations described later in this section.

Blood flow parameters are estimated from the output signal of the clutter filter. It is therefore of interest to see how the clutter filter affects such estimates. A commonly used estimator for the mean velocity in color flow imaging is calculated from an estimate of the autocorrelation

function with temporal lag $m = 1$ [12]. Mathematically, the estimator is expressed by

$$\hat{v} = \frac{c}{2f_0 T} \cdot \hat{f}_b, \quad \text{where} \quad \hat{f}_b = \arg(\hat{R}(1))/2\pi \tag{28}$$

where c is the sound velocity, f_0 is the ultrasound center frequency, T is the pulse repetition interval, $\hat{R}(1)$ is the autocorrelation estimate, and $\hat{f}_b$ is an estimate of the center frequency of the blood signal. The autocorrelation function can be estimated by the sample mean estimator

$$\hat{R}(m) = \frac{1}{M-m} \sum_{k=0}^{M-m-1} y^*(k)y(k+m)$$

$$= \frac{1}{M-m} \sum_{k=0}^{M-m-1} \sum_{j=0}^{N-1} \sum_{n=0}^{N-1} a^*(k,j)a(k+m,n)x^*(j)x(n) \tag{29}$$

and we want to investigate how the filter matrix elements $a(k,j)$ influence the mean frequency estimate $\hat{f}_b$. A set of simulations with varying mean blood frequencies was performed with signals having power spectra of the form shown in Figure 10. Both the clutter and blood signal power spectra had a Gaussian shape with parameters given in Table 3. To model the transit time effect, the bandwidth of the blood signal was proportional to the center frequency. The synthetic blood signal was generated by first calculating the Discrete Fourier Transform of a signal consisting of $512 \cdot N$ samples of complex white Gaussian noise. This signal was then multiplied by a mask corresponding to the power spectrum of the blood signal, and transformed back to the time domain. The clutter signal was calculated in a similar manner. Finally, the signal used in the simulations was the sum of these two signals and complex white Gaussian noise, giving a power spectrum as shown in Figure 10. Subdividing this signal into vectors of dimension N, we got 512 realizations of a signal with packet size N. This procedure was repeated 512 times giving a total of 262 144 realizations for each blood signal center frequency. When aliasing of the velocity estimates occurred, $\pm 2\pi$ was added to $\arg(\hat{R}(1))$ in Equation 28 to ensure that the estimates were contained in the interval $[f_b - 0.5, f_b + 0.5]$.

Figure 11 shows the bias and standard deviation of the mean frequency estimate with no clutter signal and a signal-to-noise ratio (SNR) of 30dB. The packet size is $N = 8$. The filters are designed to suppress signals with frequencies in the stopband, and therefore yield a large bias and standard deviation for Doppler frequencies within the stopband. The transition region should be as narrow as possible, and in this region we see that the polynomial regression filter yields a considerably larger bias than the other filters. The regression filter also yields bias for a

larger range of frequencies. In the passband, however, all the filters yield a negligible bias. For the FIR filter, the standard deviation in the passband is reduced when the estimate is calculated from two vectors filtered in the forward and backward direction. The improvement is largest for high frequencies since the bandwidth of the blood signal is proportional to the center frequency.

Figure 12 shows the results when the SNR is reduced to 6dB. Compared with the results for SNR=30dB, we see that the bias in the transition region and passband increases for all the filters. We also see that the regression filter has the largest bias. The difference in bias between the regression filter and the other filters is, however, much smaller for SNR=6dB which is a realistic signal-to-noise ratio. The standard deviation in the passband increases for all the filters, and the FIR filter yields a considerably higher standard deviation in the passband than the other filters. When the estimate is calculated from two vectors filtered in the forward and backward direction, the standard deviation within the passband is significantly reduced, and is comparable to the IIR and regression filter. For a linear phase FIR filter the standard deviation was approximately equal to the values obtained with a minimum phase filter applied only in the forward direction. For IIR filters there was no significant reduction of the standard deviation when filtering in both the forward and backward direction.

To see how clutter affects the mean frequency estimate, we repeated the simulations including a clutter signal denoted *Clutter signal 1*. To study the decay in performance with increased clutter level, we also performed simulations with *Clutter signal 2* where both the amplitude and bandwidth was increased. The detailed parameters for these two signals are given in Table 3. The results for *Clutter signal 1* are shown in Figure 13 where we see that they are very similar to the results with no clutter signal shown in Figure 12. This means that all the filters sufficiently suppress a clutter signal with this amplitude, bandwidth, and center frequency.

The results for *Clutter signal 2* are shown in Figure 14 where we see that the mean frequency estimates are strongly affected by this clutter signal. When studying Figure 10a, we see that the power of *Clutter signal 2* after filtering is above the thermal noise level. This low frequency signal component is an explanation for the significant negative bias in Figure 14a. The standard deviation within the passband is also large for *Clutter signal 2*. Based on the results in Figure 14 it can be concluded that none of the filters sufficiently suppress *Clutter signal 2*. The results also indicate that all the filters break down at approximately the same clutter power, bandwidth

14

and center frequency.

The influence of the packet size on the quality of the mean frequency estimator was investigated by increasing the packet size from 8 to 16. To maintain approximately the same stopband width, the dimension of the clutter space used in the regression filter was increased from 3 to 5. The other filter types were also redesigned with parameters given in Table 2 to get frequency responses similar to the regression filter as shown in Figure 10b. The results for *Clutter signal 1* are shown in Figure 15. When comparing Figure 15a and Figure 13a, we see that the range of frequencies with considerable bias is reduced when the packet size is increased from 8 to 16. This effect is related to the narrower transition region of the filters used for $N = 16$. The standard deviation of the estimates decreases with packet size since the estimates are based on a larger number of samples. The relative advantage achieved by applying the FIR filter in both directions is the same for $N = 8$ and $N = 16$.

The results for *Clutter signal 2* are shown in Figure 16 where we see that all the filters have similar performance and yield a small negative bias for Doppler frequencies within the passband. We also see that the standard deviation is significantly increased for the highest Doppler frequencies compared to the results for *Clutter signal 1* shown in Figure 15. The filters do not completely suppress the clutter signal, but they perform significantly better than the filters used for packet size $N = 8$. An explanation for this is the wider stopbands of the filters used for $N = 16$.

7   Discussion and Conclusions

The frequency response of FIR filters is improved when a nonlinear phase response is allowed. The commonly used autocorrelation estimates do not depend on the phase response, so a filter with non-linear phase response can safely be chosen. A significant reduction of the variance of the mean frequency estimator was obtained by filtering with a minimum phase filter in both the forward and backward direction. Linear phase FIR filters have symmetric impulse responses, and nothing is gained by filtering in both the forward and backward direction. A large gain in performance can thus be obtained by using a minimum phase filter instead of a linear phase filter.

For short signal lengths, the frequency response for IIR filters is highly dependent on the initialization technique. We found that the best frequency response for IIR filters is obtained when projection initialization is used. The other initialization techniques do not provide a sufficient stopband width for clutter rejection.

Within the class of regression filters, polynomial basis functions were shown to provide useful frequency responses. Polynomial regression filters and projection initialized IIR filters of the same order have almost identical properties. An explanation for this is that the output vector for both filters is projected into the orthogonal complement of a subspace with low frequency basis functions.

Among the three filter classes, polynomial regression filters and projection initialized IIR filters have the best frequency response. For equal stopband width, the transition regions were narrower than for FIR filters. An advantage of FIR filters is the greater flexibility in specifying the filter cut-off frequency, which is also independent of the packet size. To increase the stopband width for projection initialized IIR filters, it was better to increase the filter order than to increase the steady state cut-off frequency.

Simulations were performed to investigate how the bias and standard deviation of the mean frequency estimator were affected by the clutter filters. The simulations showed that for all the filter types, the frequency response is a reliable indicator of the range of blood velocities that can be measured with good quality. For Doppler frequencies within the passband, there was no significant differences in the bias produced by the different filters for realistic noise and clutter levels. The different filter types break down at approximately the same clutter level. IIR and regression filters provide a larger number of output samples than FIR filters provide. The simulations showed that this larger number of samples reduces the variance of the mean frequency estimator within the passband compared to FIR filters. By using a minimum phase FIR filter in both the forward and backward direction, there was, however, no significant difference in variance between the three filter classes. The simulations also showed that the relative performance between the filters did not change significantly with packet size.

When using projection initialization, IIR filters have a computational complexity similar to that of regression filters. The computational complexity is considerably smaller for FIR filters. However, if minimum estimator variance is desired, the FIR filter should be applied twice, and

more computations are needed for the autocorrelation estimate.

8 Acknowledgements

References

[1] R. H. Fletcher and D. W. Burlage, "An initialization technique for improved MTI performance in phased array radars," *Proc. IEEE*, vol. 60, pp. 1551–1552, Dec. 1972.

[2] E. S. Chornoboy, "Initialization for improved IIR filter performance," *IEEE Trans. Signal Process.*, vol. 40, pp. 543–550, Mar. 1992.

[3] A. P. Kadi and T. Loupas, "On the performance of regression and step-initialized IIR clutter filters for color Doppler systems in diagnostic medical ultrasound," *IEEE Trans. Ultrason., Ferroelect., Freq. Contr.*, vol. 42, pp. 927–937, Sept. 1995.

[4] T. W. Parks and C. S. Burrus, *Digital Filter Design.* John Wiley & Sons, Inc., 1987.

[5] A. P. G. Hoeks, J. J. W. van de Vorst, A. Dabekaussen, P. J. Brands, and R. S. Reneman, "An efficient algorithm to remove low frequency Doppler signals in digital Doppler systems," *Ultrason. Imag.*, vol. 13, pp. 135–144, Apr. 1991.

[6] H. Torp, "Clutter rejection filters in color flow imaging: A theoretical approach," *IEEE Trans. Ultrason., Ferroelect., Freq. Contr.*, vol. 44, pp. 417–424, Mar. 1997.

[7] M. A. Shariati, J. H. Dripps, and W. N. McDicken, "Deadbeat IIR based MTI filtering for color flow imaging systems," in *1993 IEEE Ultrasonics Symposium Proceedings*, vol. 2, pp. 1059–1063, Oct. 1993.

[8] R. B. Peterson, L. E. Atlas, and B. K. W., "A comparison of IIR initialization techniques for improved color Doppler wall filter performance," in *1994 IEEE Ultrasonics Symposium Proceedings*, vol. 3, pp. 1705–1708, Nov. 1994.

[9] L. Thomas and A. Hall, "An improved wall filter for flow imaging of low velocity flow," in *1994 IEEE Ultrasonics Symposium Proceedings*, vol. 3, pp. 1701–1704, Nov. 1994.

[10] J. S. Lim and A. V. Oppenheim, eds., *Advanced Topics in Signal Processing.* Prentice Hall, Inc., 1988.

[11] J. G. Proakis and D. G. Manolakis, *Digital Signal Processing, Principles, Algorithms, and Applications.* Macmillan Publishing Company, second ed., 1992.

[12] C. Kasai, K. Namekawa, A. Koyano, and R. Omoto, "Real-time two-dimensional blood flow imaging using an autocorrelation technique," *IEEE Trans. Sonics Ultrason.*, vol. 32, pp. 458–464, May 1985.

[13] P. P. Vaidyanathan, *Multirate Systems and Filter Banks.* Prentice Hall, Inc., 1993.

Figure captions

Figure 1:

Design parameters for a high pass filter.

Figure 2:

Frequency responses for linear and minimum phase FIR filters of order 5.

Figure 3:

The transient signal for the Butterworth, Chebyshev, and Elliptic filters shown in Figure 5. The input signal was $\sin(n\pi/5 + \pi/4)$.

Figure 4:

Mirroring of the input sequence around the first sample.

Figure 5:

Frequency responses for Butterworth, Chebyshev, and elliptic filters with different initialization techniques. Packet size $N = 8$.

Figure 6:

Frequency responses for the Chebyshev filter with different initialization techniques when the input signal is mirrored. Packet size $N = 8$.

Figure 7:

Projection initialized Chebyshev responses as a function of order and steady state cut-off frequency. Packet size $N = 8$.

Figure 8:

Frequency responses for regression filters with sinusoidal basis vectors. Clutter space dimension $K = 3$, and packet size $N = 8$.

Figure 9:

(a) Frequency responses for polynomial regression filters with packet size $N = 8$. The clutter space dimension is indicated on each curve. (b) Frequency responses for filters described in Equation 27 with $c_0 = c_1 = 1$ and c_2 equal to 0.25, 0.5 and 0.75 are plotted with dashed lines.

Figure 10:

Comparison of frequency responses of polynomial regression filters, projection initialized IIR Chebyshev filters, and a minimum phase FIR filters. (a) Packet size $N = 8$. (b) Packet size $N = 16$. The design parameters are given in Table 2.

Figure 11:

(a) Bias and (b) standard deviation of the mean frequency estimate for the three different filters in Figure 10a. The frequency of the polynomial regression filter is plotted to indicate the passbands of the filters. No clutter is present and the SNR is 30dB. The packet size is $N = 8$.

Figure 12:

(a) Bias and (b) standard deviation of the mean frequency estimate for the three different filters in Figure 10a. The frequency of the polynomial regression filter is plotted to indicate the passbands of the filters. No clutter is present and the SNR is 6dB. The packet size is $N = 8$.

Figure 13:

(a) Bias and (b) standard deviation of the mean frequency estimate with *Clutter signal 1* for the three different filters in Figure 10a. The frequency of the polynomial regression filter is plotted to indicate the passbands of the filters. The SNR is 6dB and the packet size is $N = 8$.

Figure 14:

(a) Bias and (b) standard deviation of the mean frequency estimate with *Clutter signal 2* for the three different filters in Figure 10a. The frequency of the polynomial regression filter is plotted to indicate the passbands of the filters. The SNR is 6dB and the packet size is $N = 8$.

Figure 15:

(a) Bias and (b) standard deviation of the mean frequency estimate with *Clutter signal 1* for the three different filters in Figure 10a. The frequency of the polynomial regression filter is plotted to indicate the passbands of the filters. The SNR is 6dB and the packet size is $N = 16$.

Figure 16:

(a) Bias and (b) standard deviation of the mean frequency estimate with *Clutter signal 2* for the three different filters in Figure 10a. The frequency of the polynomial regression filter is plotted to indicate the passbands of the filters. The SNR is 6dB and the packet size is $N = 16$.

Table captions

Table 1:

Optimum linear and minimum phase FIR filters of order 5. Design parameters: minimum $\omega_s = 0.02\pi$, maximum $d_p = 0.5$dB, and minimum $d_s = -80$dB

Table 2:

Filter design parameters.

Table 3:

Parameters for the simulated spectra. Clutter signal 1 is plotted with a dashed line in Figure 10, while Clutter signal 2 is plotted with a solid line.
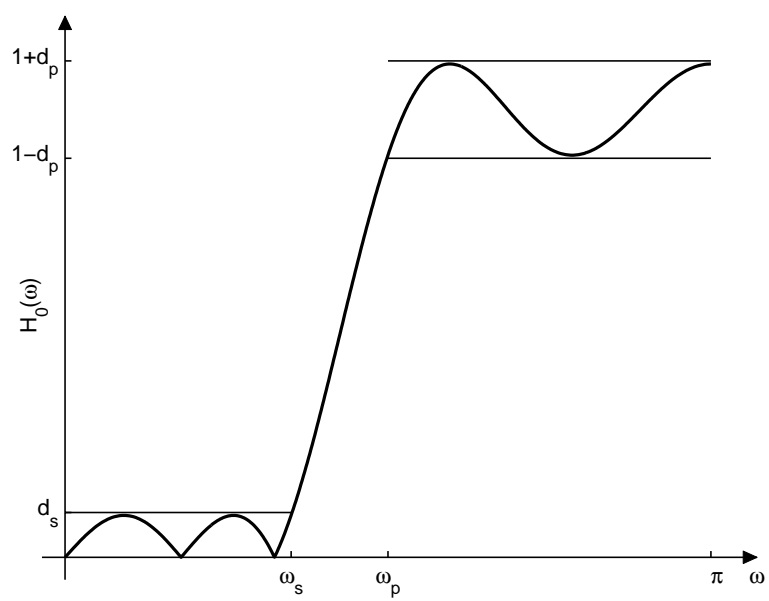
Figure 1
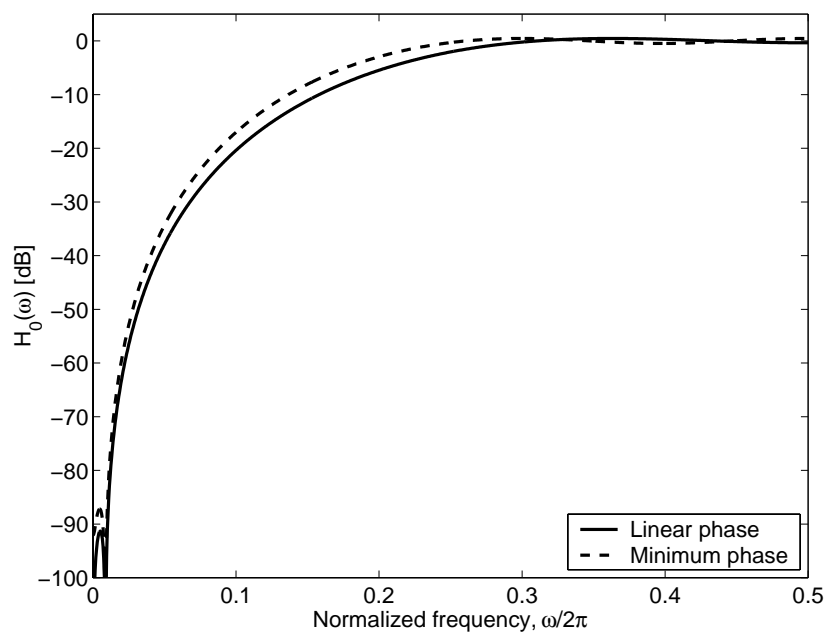
Figure 2
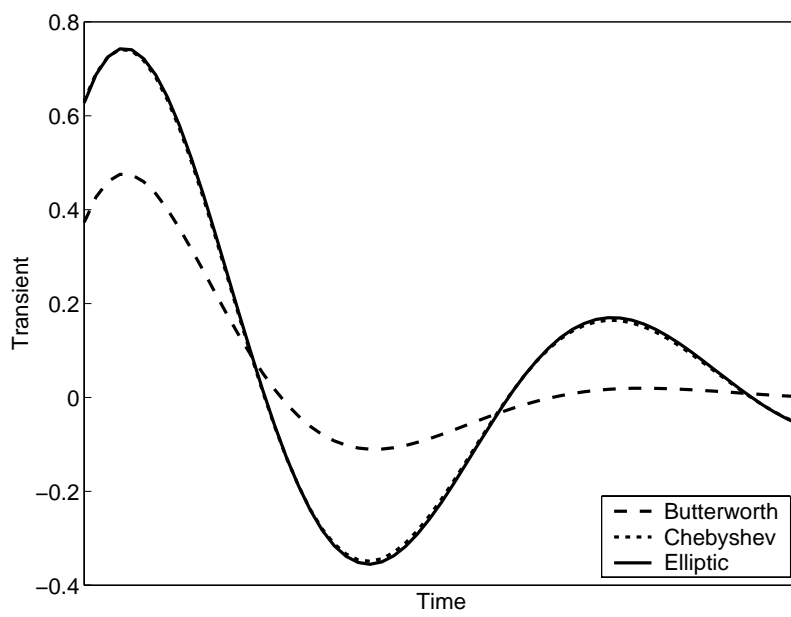
Figure 3

Figure 4

Figure 5

28
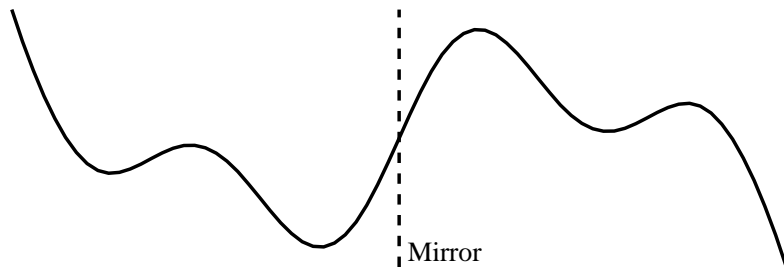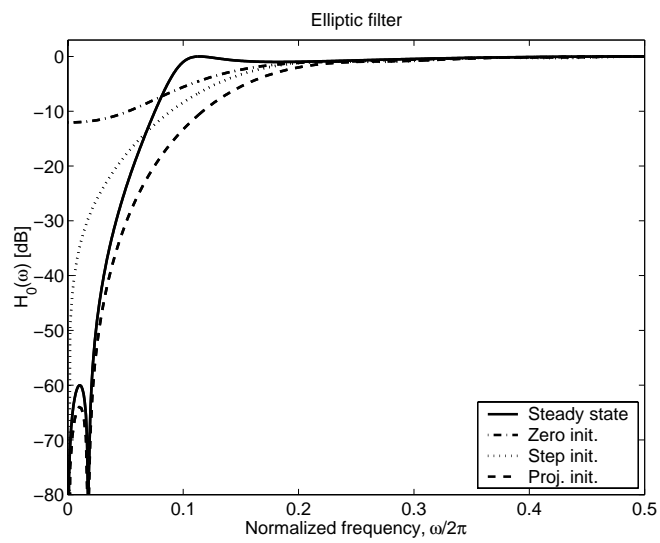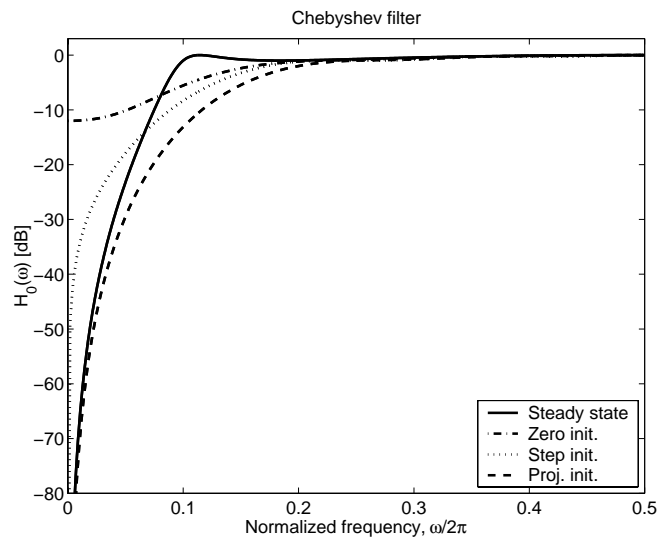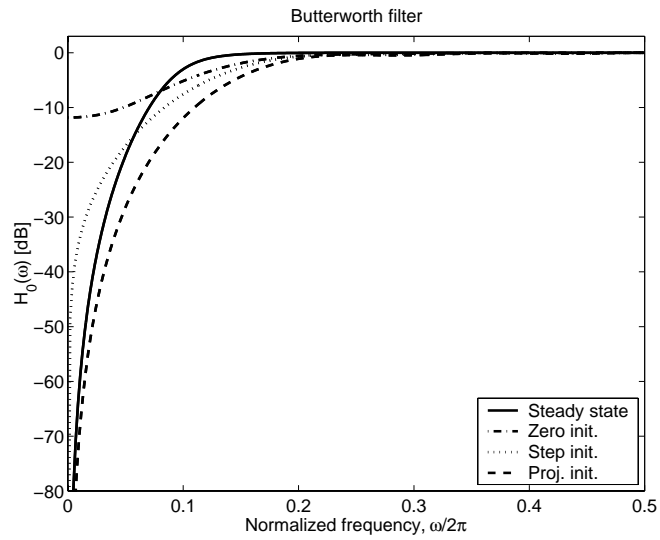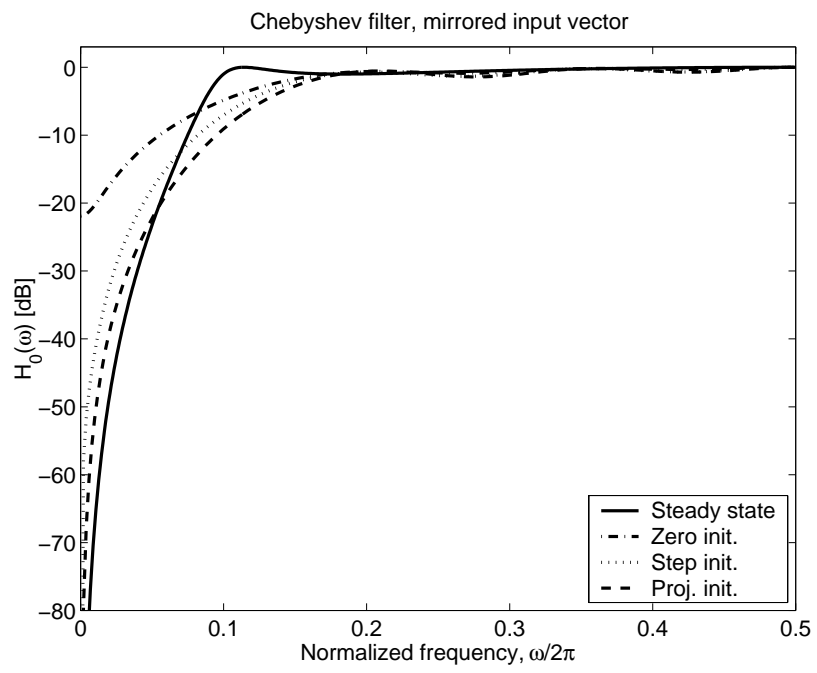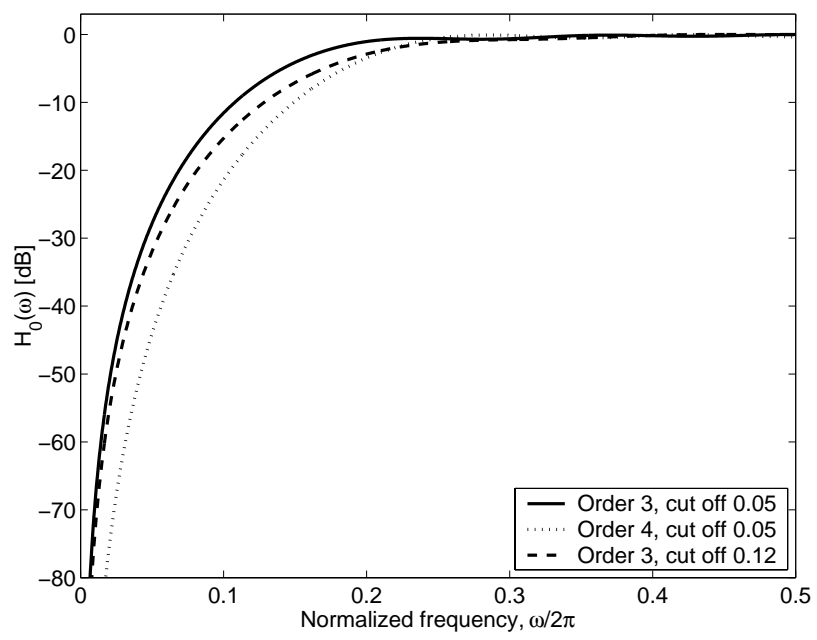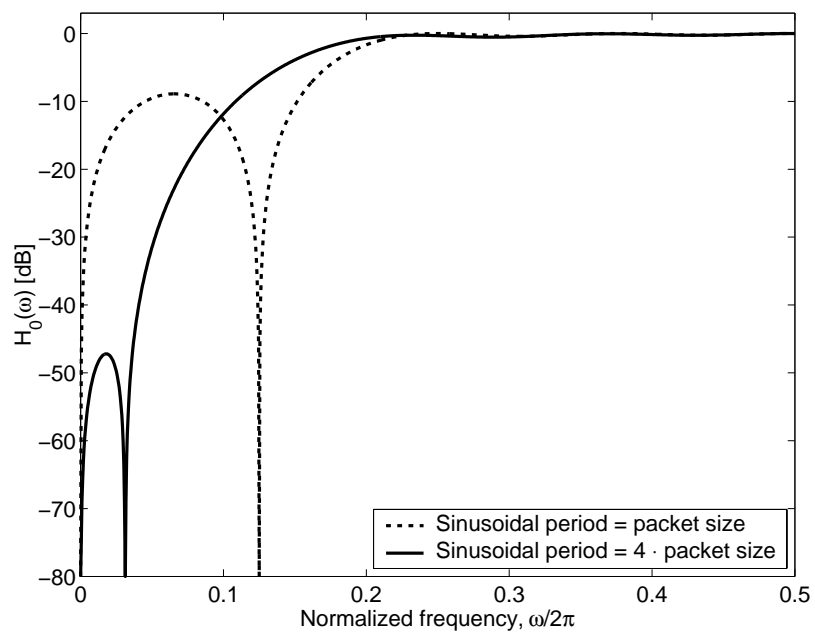
Figure 6

Figure 7

Figure 8
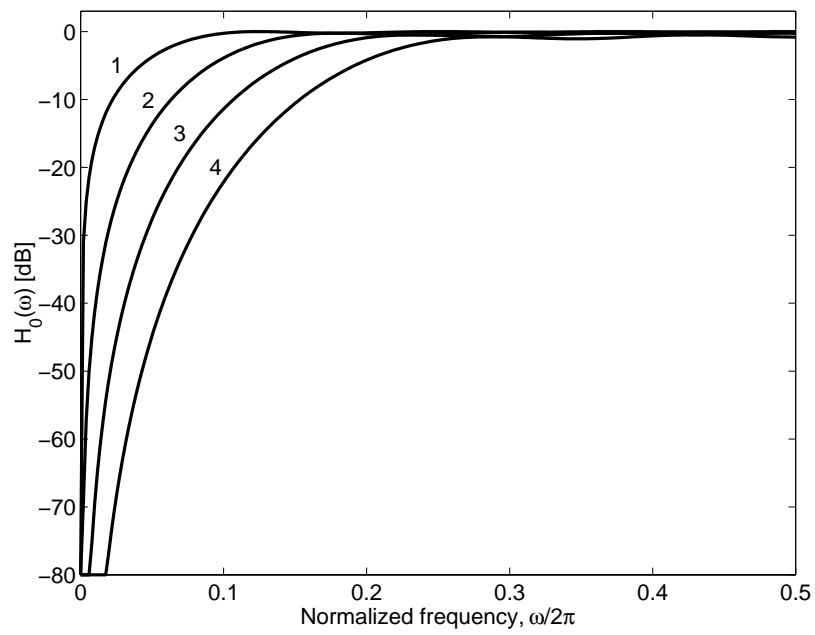
(a)
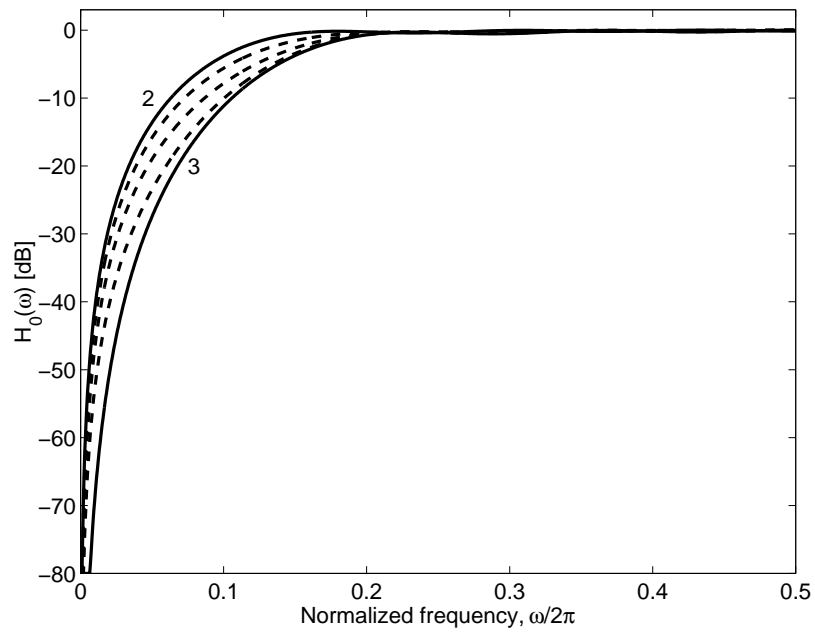
(b)

Figure 9
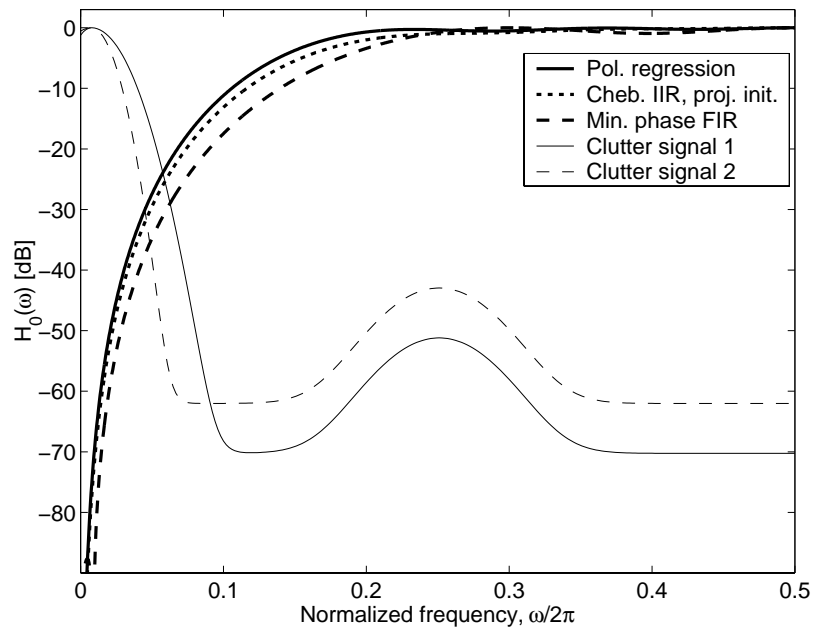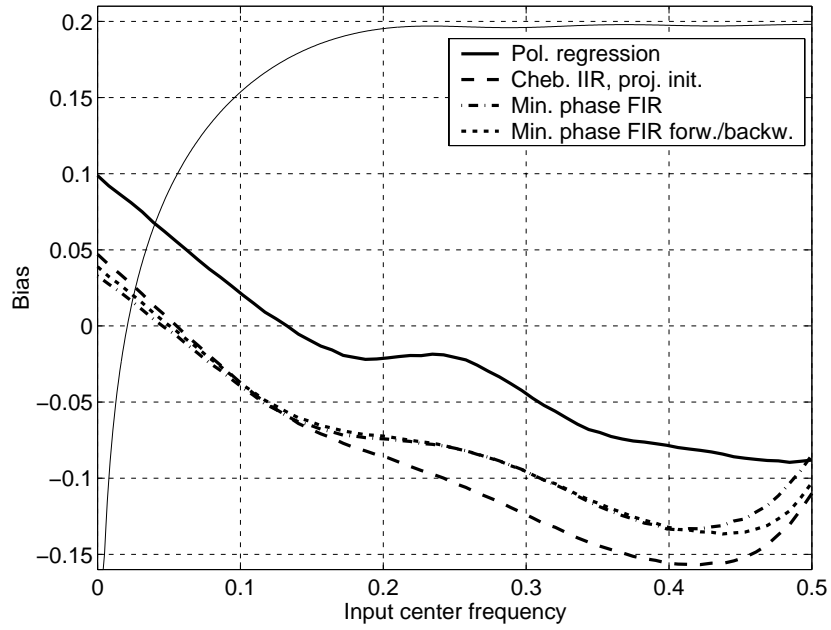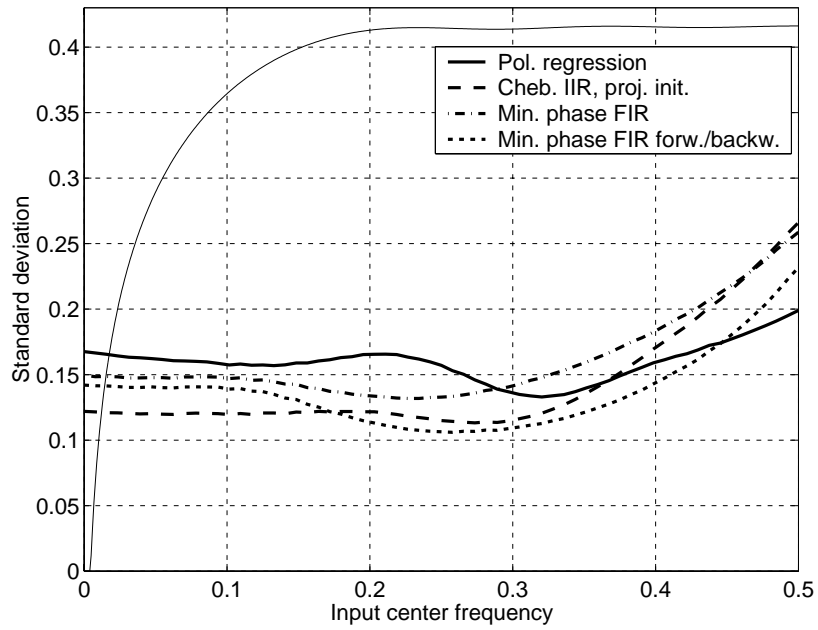
(a)
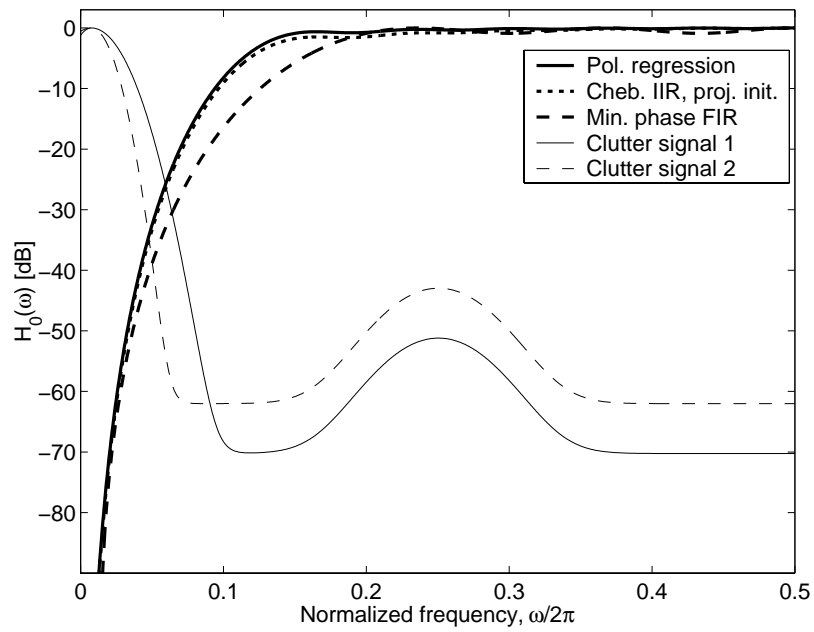
(b)

Figure 10
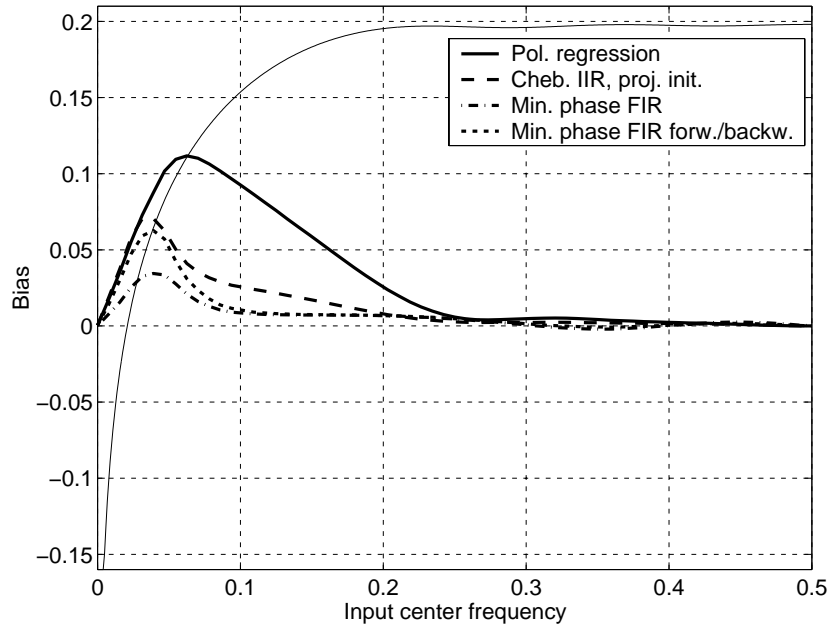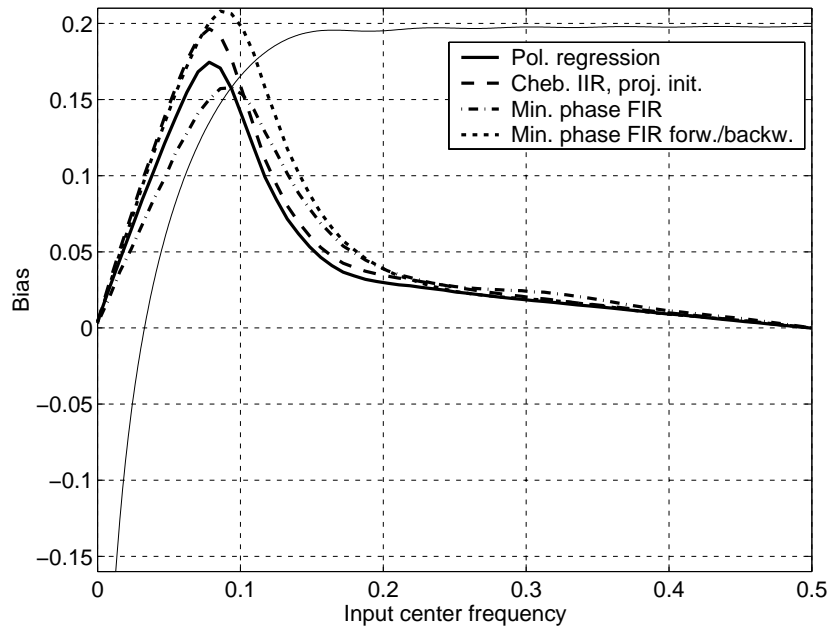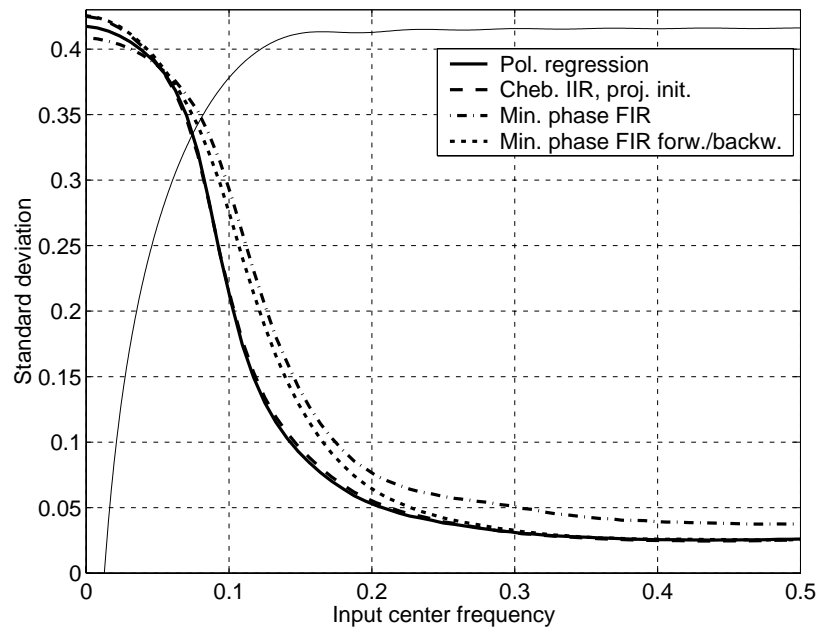
(a)
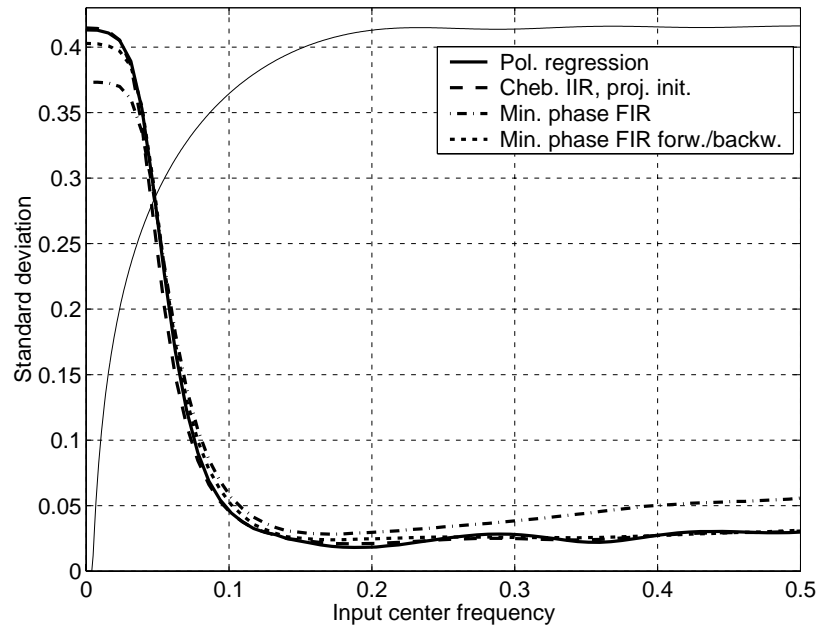
(b)

Figure 11
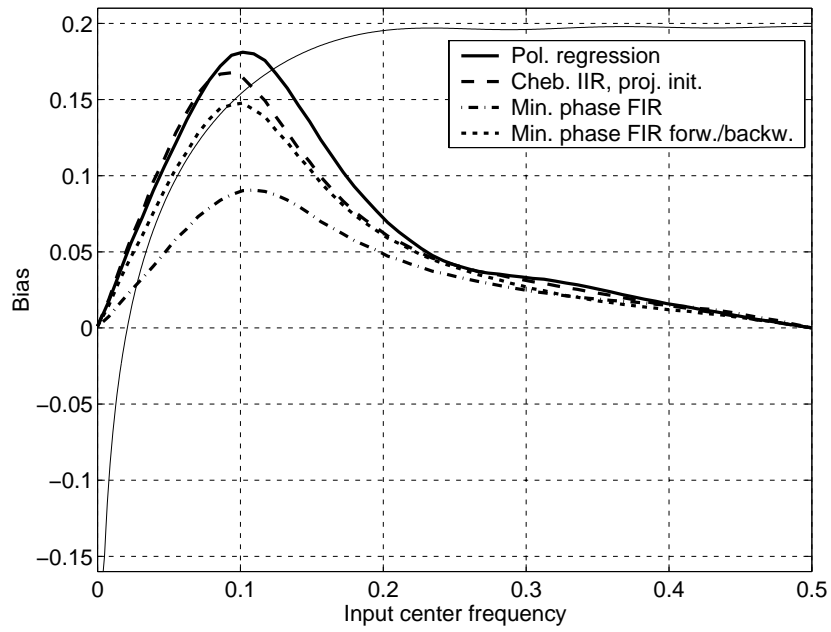
(a)
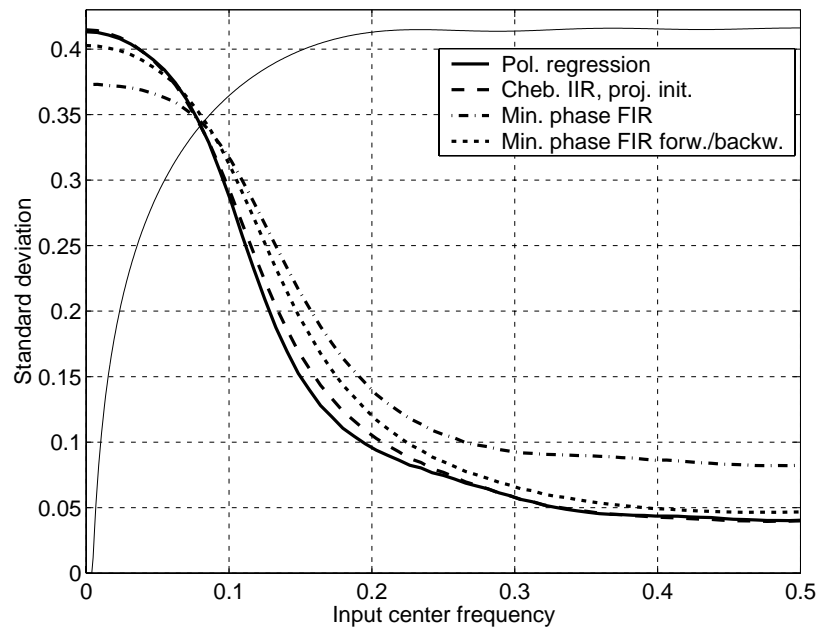
(b)

Figure 12
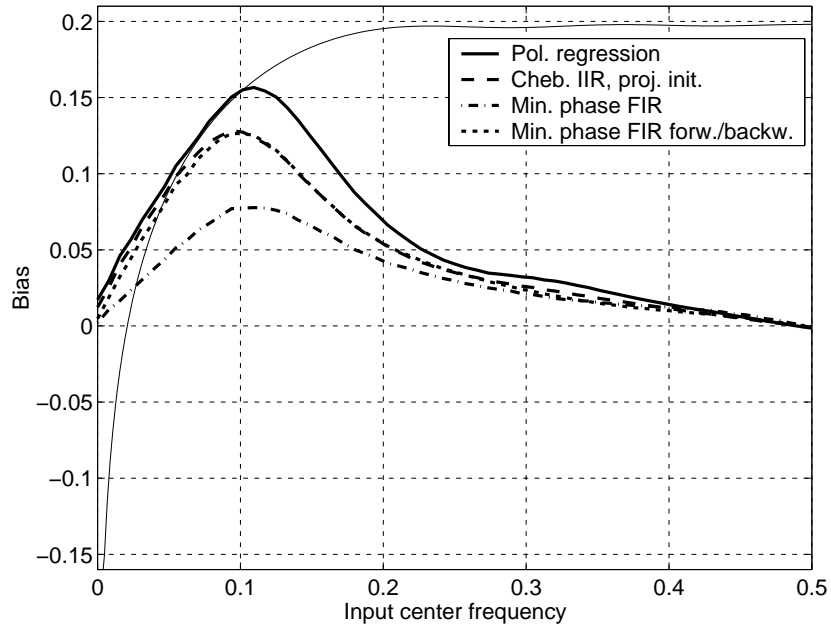
(a)
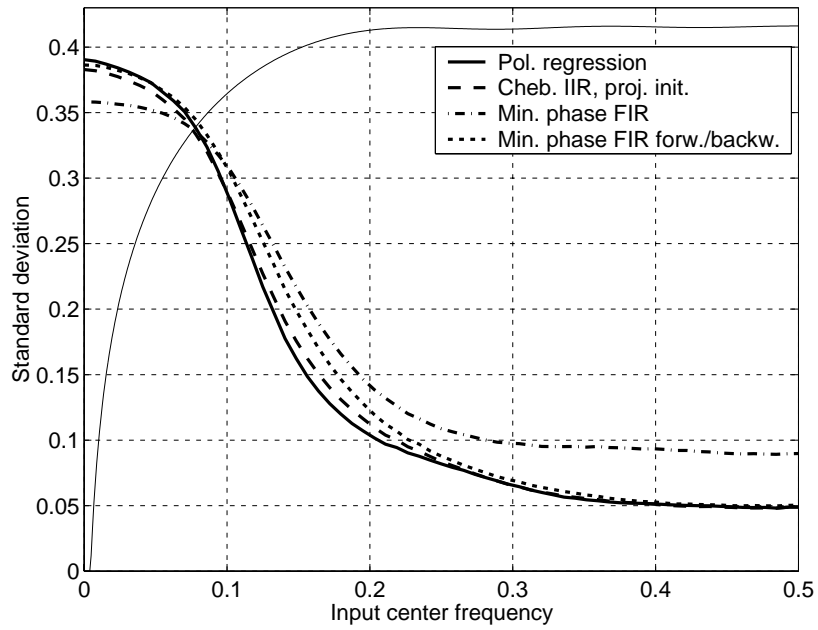
(b)

Figure 13

(a)

(b)

Figure 14
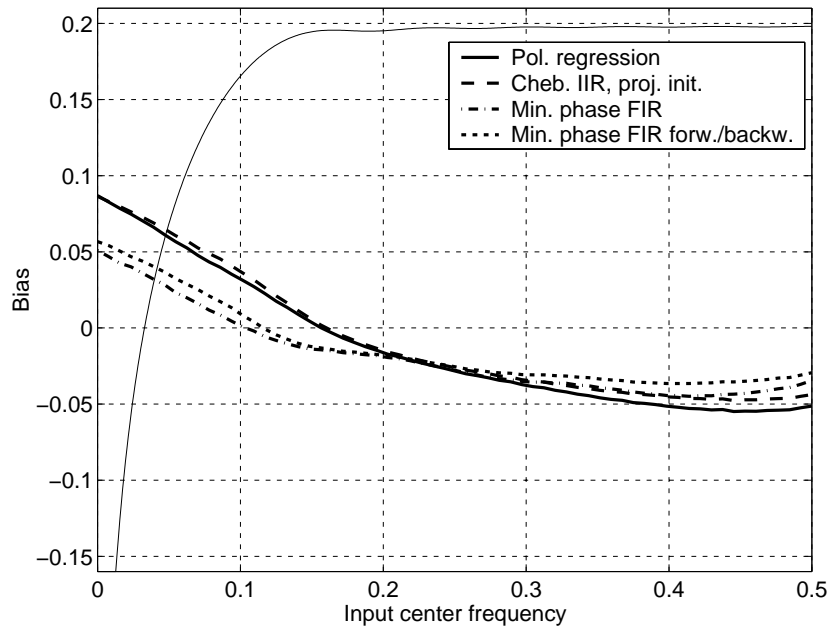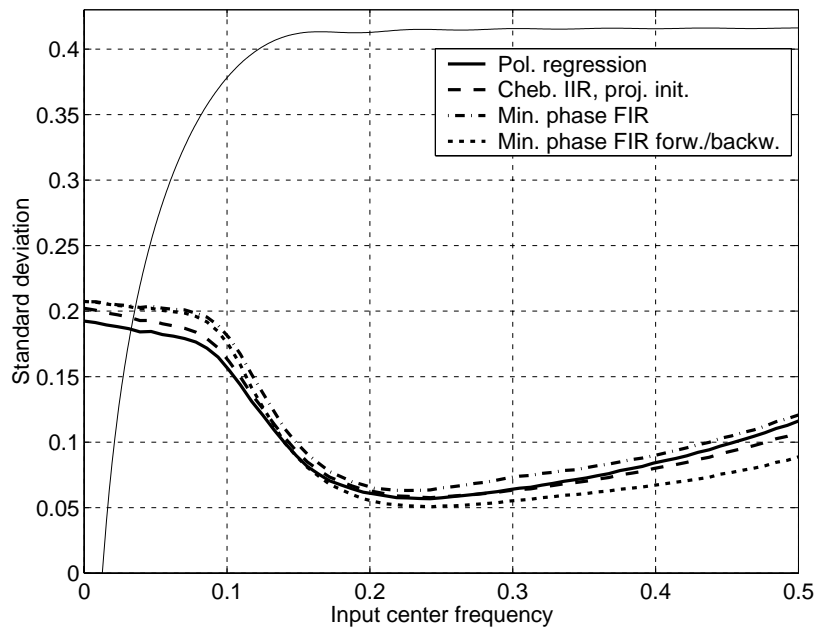
(a)

(b)

Figure 15

(a)

(b)

Figure 16

	Min. phase	Lin. phase
ω_p	0.49π	0.58π
d_s [dB]	-87dB	-91dB

Table 1

Packet size $N = 8$		Packet size $N = 16$	
Filter type	Parameter	Filter type	Parameter
Proj. init. IIR Chebyshev	Order $= 3$ $\omega_p = 0.2\pi$ $d_p = 0.5$dB	Proj. init. IIR Chebyshev	Order $= 5$ $\omega_p = 0.1\pi$ $d_p = 0.5$dB
Min. phase FIR	Order $= 5$ Minimum $\omega_s = 0.02\pi$ Maximum $d_p = 0.5$dB Minimum $d_s = -80$dB Achieved $d_s = -87$dB Achieved $\omega_p = 0.49\pi$	Min. phase FIR	Order $= 8$ Minimum $\omega_s = 0.03\pi$ Maximum $d_p = 0.5$dB Minimum $d_s = -80$dB Achieved $d_s = -92$dB Achieved $\omega_p = 0.40\pi$
Pol. reg.	Clut. space dim. $= 3$	Pol. reg.	Clut. space dim. $= 5$

Table 2

	Clutter signal 1	Clutter signal 2
Clutter-to-flow-signal power ratio, CSR	40dB	50dB
Clutter signal RMS Bandwidth, B_c	0.01PRF	0.015PRF
Clutter signal center frequency, f_c	0.0075PRF	0.0075PRF
Blood signal center frequency, f_b	0 to 0.5PRF	0 to 0.5PRF
Blood signal RMS Bandwidth, B_b	$0.1f_b$	$0.1f_b$

Table 3